Vacuum-excited surface plasmon polaritons

Wade Naylor*

International College and Department of Physics, Interdisciplinary Research Building, Osaka University, Toyonaka, Osaka 560-0043, Japan

(Received 19 May 2014; revised manuscript received 11 March 2015; published 6 May 2015)

We separate Maxwell's equations for background media that allow for both electric and magnetic time dependence in a generalized Lorenz gauge. In a process analogous to the dynamical Casimir effect (DCE) we discuss how surface plasmon polaritons (SPPs) can be created out of vacuum via the time-dependent variation of a dielectric and magnetic insulator at a metal interface for TM and TE branches, respectively. We suggest how to extend currently proposed DCE experiments to set up and detect these excitations. Numerical simulations (without any approximation) indicate that vacuum-excited SPPs can be of a similar magnitude to the photon creation rate in such experiments. Potential benefits of detecting vacuum-excited SPPs, as opposed to DCE photons, are that parametric enhancement does not require a sealed cavity in the axial direction and the detection apparatus might be able to use simple phase-matching techniques. For the case of constant permeability μ, TM branch SPPs and photons do not suffer from detuning and attenuation like TE photons.

DOI: 10.1103/PhysRevA.91.053804 PACS number(s): 42.50.Ct, 42.50.Pq, 42.50.Lc, 42.60.Da

I. INTRODUCTION

Particle creation via the Schwinger effect [1], in expanding universes [2], or from black-hole evaporation [3] has yet to be confirmed.[1] However, a related effect known as the dynamical Casimir effect (DCE), first discussed by Moore [7], is within experimental reach. For the parametric oscillations of a mirror contained in a cavity the number of photons created is proportional to $\sinh^2(2\omega t\, v/c)$ (e.g., see [8]), where v is the wall velocity and c is the speed of light. To overcome the fact that the mechanical properties of the material usually imply $v/c \ll 1$, there have been proposals other than mechanical oscillations. Modulating a dielectric medium using a laser also leads to particle creation by varying the optical path length of the cavity (e.g., see [9]). There are experiments in progress in three-dimensional centimeter-sized (microwave) cavities [10] in which a laser is used to modulate the surface conductivity. Other methods use illuminated superconducting boundaries [11], and recently, time-varied inductance effects in one-dimensional quantum circuits have already demonstrated vacuum squeezing [12,13]. Rotating analogs have also been investigated [14].

In this article we explore the possibility of the creation of vacuum-excited surface plasmon polaritons (SPPs) and how they might be detected. In Fig. 1 a pulsed laser of an appropriate frequency can be used to vary the time dependence of a dielectric. The crystal can also be placed in a superconducting cavity (not shown) to suppress thermal excitations and add to parametric enhancement of the photon creation rate. SPPs are, by definition, damped modes of oscillation in the perpendicular direction and therefore are affected only by the transverse dimensions. This means that only the transverse dimensions need to be enclosed to obtain parametric enhancement, which might be a potential benefit experimentally.

A telltale signature of the creation of SPPs would be *an increase in emitted power at position* θ_i when coupled to a phase-matched prism at one end of the semiconductor-metal (SM) interface.[2] This is in stark contrast to the usual SPP generation method and detection (e.g., see [15]), in which a decrease in emitted power at θ_i occurs via illumination of the prism. As well as SPPs, TE and TM photon pair creation is also expected; however, these are at different frequencies and would not couple to the prism and would further require a sealed cavity (we further discuss detection methods later).

The fact that SPPs can be excited from vacuum fluctuations besides photons is much like SPPs in the static Casimir force [16] for a metal-insulator-metal (MIM) heterostructure. We essentially generalize this idea to the dynamical case for the simpler single interface, a semiconductor-metal (SM) interface, and show that the time modulation of a dielectric leads not only to two-photon pair creation processes but also to vacuum-excited SPPs that are comparable to the photon creation rate, under certain conditions. This may well have important consequences for experiments currently trying to detect pair-created photons. Theoretically, a dynamical Casimir effect for a single interface arises from the analogy that a single moving boundary emits DCE radiation, even though there is no Casimir force [8].

The outline of this article is as follows. In Sec. II we give details of the theory behind time-dependent surface plasmons, while in Sec. III we use a generalized plasma model to obtain analytic expressions for the SPP dispersion relations. In Sec. IV we discuss how to numerically evaluate the particle creation rate via a full separation of variables without any approximation, while in Sec. V we propose possible detection schemes. We conclude in Sec. VI. Extra material is left for appendices: information related to Maxwell's equations for time-dependent dielectrics (Appendix A), the Hertz vector approach to separation (Appendix B), and a comparison of the exact separation of variables with the instantaneous basis approach (Appendix C).

*naylor@phys.sci.osaka-u.ac.jp

[1]This excludes analog setups (e.g., see [4]). In particular, for graphene there are some promising proposals [5,6] to observe a $(2+1)$-dimensional Schwinger effect.

[2]Here we consider a semiconductor semispace. Usually, in plasmonics an insulator-metal (IM) interface is assumed (e.g., see [15]).

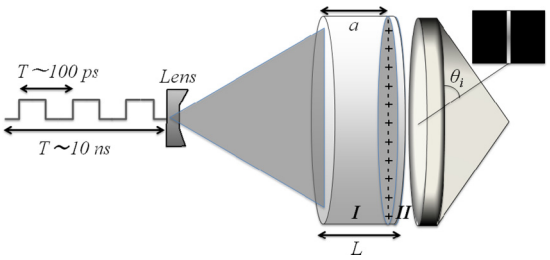

FIG. 1. (Color online) A pulse laser train of order 10–100 pulses (repeating ~10 ms) uniformly irradiates (via a lens) a semiconductor-metal (SM) interface of radius R, composed of a dielectric of thickness a, region I, at a thin metal (e.g., silver) interface of thickness $(L-a) \ll L$, region II. Vacuum-excited SPPs $(-+-+-+)$ are detected using a phase-matched prism placed to the right of region II.

II. THEORY

Our theoretical starting point is the following Lagrangian (from which Maxwell's equations can be derived):

$$\mathcal{L} = \frac{1}{2}\varepsilon(t)\left(\frac{\partial}{\partial t}\Phi\right)^2 - \frac{1}{2}\frac{1}{\mu(t)}(\nabla\Phi)^2 - \frac{1}{2}m^2(t)\Phi^2 \qquad (1)$$

($\varepsilon_0 = \mu_0 = 1$). In the above we assume that the electric permittivity and magnetic permeability are time dependent but piecewise constant in space: $\nabla\mu = \nabla\varepsilon = 0$. Φ represents a TM field with generalized Neumann boundary conditions in a cavity, and the TE case (swapping $\varepsilon \leftrightarrow \mu$) is represented by Ψ with Dirichlet boundary conditions (e.g., see [17]). This Lagrangian is useful because the standard canonical Hamiltonian can be constructed [18], where the mass term $m^2(t)$ represents the coupling of light to a time-dependent boundary (m^2 can also arise from considering an electron plasma).

A convenient way to separate Maxwell's equations is to use Hertz vectors, developed by Nisbet [19] for nondispersive inhomogeneous media. However, here we generalize to the case of a constant isotropic but time-dependent medium. It is possible to show (see Appendix A) that Maxwell's equations separate as

$$\begin{aligned}\varepsilon(t)\partial_t(\mu(t)\partial_t\mathbf{\Pi}_e) - \nabla^2\mathbf{\Pi}_e = 0,\\ \mu(t)\partial_t(\varepsilon(t)\partial_t\mathbf{\Pi}_m) - \nabla^2\mathbf{\Pi}_m = 0,\end{aligned} \qquad (2)$$

where we use a generalized Lorenz gauge (also discussed in Appendix A):

$$\mu(t)\partial_t(\varepsilon(t)A_0) + \nabla\cdot\mathbf{A} = 0 \qquad (3)$$

[see [19,20] and Eq. (A6)]. In the above we have assumed both zero permanent polarization and magnetization ($\mathbf{P}_0 = \mathbf{M}_0 = 0$) as well as zero bulk charges and currents ($\rho = 0, \mathbf{J} = 0$), although these can also be included in the Hertz method. Note the Lagrangian in Eq. (1) leads to the equations of motion for $\mathbf{\Pi}_e$ in Eq. (2) [$\mathbf{\Pi}_m$ is obtained by swapping $\mu \leftrightarrow \varepsilon$ in Eq. (1); see Appendix A]. This approach generalizes other work [9,20] which considered only time-dependent ε or μ. Further work for nondispersive, inhomogeneous, conducting and time-dependent media, $\varepsilon(\mathbf{r},t)$ and $\mu(\mathbf{r},t)$, will be presented elsewhere.

Before quantizing the SPP modes we first need to find the classical solutions for a single interface (between two media) that lead to SPPs. Writing the electric and magnetic fields in terms of Hertz vectors:

$$\begin{aligned}\mathbf{E} &= \frac{1}{\varepsilon}\nabla\times(\nabla\times\mathbf{\Pi}_e) - \mu_0\nabla\times\partial_t\mathbf{\Pi}_m,\\ \mathbf{B} &= \mu\nabla\times\frac{\partial\mathbf{\Pi}_e}{\partial t} + \mu_0\nabla\times(\nabla\times\mathbf{\Pi}_m),\end{aligned} \qquad (4)$$

allowing one to easily isolate TE and TM modes (see Appendix B).

In what follows we take two half spaces in the $\hat{\mathbf{z}}$ direction, where region I (the semiconductor slab) is a semiconductor (S) and region II is a metal (M) such as silver, creating an SM interface.

In our proposed setup $\varepsilon_1(t)$ varies from a minimum to maximum value, and $\varepsilon_2 < 0$ remains constant (although for now it will be left more general). To make explicit the utility of the Hertz vector method we shall consider the radial propagation of SPPs in a cylindrical cavity with coordinates (ρ,θ,z), sectional radius $\rho = R$, and length L (see Fig. 1).

Using the Hertz potentials (2) and assuming from symmetry that $\mathbf{\Pi}_m = \Psi\hat{\mathbf{z}}$ for TE and $\mathbf{\Pi}_e = \Phi\hat{\mathbf{z}}$ for TM modes, the separation of variables,

$$\begin{aligned}\Psi(\mathbf{x},t) &= \sum_{\mathbf{l}}\psi_{\mathbf{l}}(\mathbf{x})q^m_{\mathbf{l}}(t),\\ \Phi(\mathbf{x},t) &= \sum_{\mathbf{l}}\phi_{\mathbf{l}}(\mathbf{x})q^e_{\mathbf{l}}(t),\end{aligned} \qquad (5)$$

with $\mathbf{l} = (n,p,l)$, leads to the following wave equation (e.g., see [21]):

$$\nabla^2\psi_{\mathbf{l}}(\mathbf{x}) + \varepsilon(t)\mu(t)\omega^2_{\mathbf{l}}(t)\psi_{\mathbf{l}}(\mathbf{x}) = 0, \qquad (6)$$

with the replacement $\psi_{\mathbf{l}} \to \phi_{\mathbf{l}}$ for TM modes. This equation satisfies the standard orthonormality conditions:

$$\int_{-\infty,0}^{\infty,L} d^3\mathbf{x}\,\psi_{\mathbf{l}}(\mathbf{x})\psi_{\mathbf{n}}(\mathbf{x}) = (\psi_{\mathbf{l}},\psi_{\mathbf{n}}) = \delta_{\mathbf{ln}}, \qquad (7)$$

where the $(-\infty,\infty)$ bounds on the integral are for SPPs and those with $(0,L)$ are for the photon branch (see below). We then find that the time-dependent part satisfies

$$\ddot{q}^m_{\mathbf{l}} + \frac{\dot{\varepsilon}}{\varepsilon}\dot{q}^m_{\mathbf{l}} + \omega^2_{m\mathbf{l}}q^m_{\mathbf{l}} = 0, \qquad (8)$$

$$\ddot{q}^e_{\mathbf{l}} + \frac{\dot{\mu}}{\mu}\dot{q}^e_{\mathbf{l}} + \omega^2_{e\mathbf{l}}q^e_{\mathbf{l}} = 0, \qquad (9)$$

where the superscripts m and e are for TE and TM modes, respectively. Importantly, we see that for setups with only dielectrics present, $\mu_{\mathrm{I,II}} = \text{const}$, the TM mode functions are simple Mathieu-like equations with natural frequency given by $\omega_{e\mathbf{l}}$. On the other hand, for TE modes, the presence of $\dot{\varepsilon}$ and $\dot{q}_m$ leads to a detuning via $\tilde{\omega}_{m\mathbf{l}}$ [see Eq. (37)] and also losses for $\dot{\varepsilon} > 0$ [21].

The conjugate momentum $\mathcal{P}_m = \partial\mathcal{L}/\partial t$ can be found from Eq. (1) along with the separation ansatz and orthonormality relations, implying

$$\mathcal{P}_m(\mathbf{x},t) = \varepsilon(t)\sum_{\mathbf{l}}\psi_{\mathbf{l}}(\mathbf{x})p^m_{\mathbf{l}}(t), \qquad (10)$$

and via a Legendre transform we find the time-dependent Hamiltonian for each mode $\mathbf{l}$ (TE):

$$H_{\mathbf{l}}^{m} = \varepsilon^{-1}\frac{\left(p_{\mathbf{l}}^{m}\right)^{2}}{2} + \frac{\varepsilon}{2}\omega_{\mathbf{l}}^{2}(t)\left(q_{\mathbf{l}}^{m}\right)^{2}, \tag{11}$$

where the conjugate mode momentum is defined by[3]

$$p_{\mathbf{l}}^{m} = \dot{q}_{\mathbf{l}}^{m}. \tag{12}$$

Given the equal-time commutation relations, $[\hat{q}_{\mathbf{l}}, \hat{p}_{\mathbf{n}}] = i\delta_{\mathbf{ln}}$, we get back the equation of motion, Eq. (8), from the above Hamiltonian. A similar analysis applies to TM modes, $\Phi, \mathcal{P}_e$, and hence we can quantize each degree of freedom (Φ, Ψ). In the above we rescaled the coordinates as $q_{\mathbf{l}}^{m} \to \varepsilon^{-1/2} q_{\mathbf{l}}^{m}$ for TE and would need $q_{\mathbf{l}}^{e} \to \mu^{-1/2} q_{\mathbf{l}}^{e}$ for TM modes (see below). In terms of these creation and annihilation operators we see squeezing terms in the Hamiltonian [21].

SPP and photon branches

To investigate SPPs for a single interface the ansatz

$$\Phi_{\rm sp}(\mathbf{x},t) = \begin{cases} A_1 e^{\kappa_{1l}(z-a)} r_{\rm np}(\mathbf{x}_\perp), & z < a\,;\varepsilon_1,\mu_1, \\ A_2 e^{-\kappa_{2l}(z-a)} r_{\rm np}(\mathbf{x}_\perp), & z > a\,;\varepsilon_2,\mu_2, \end{cases} \tag{13}$$

leads to the following "time-dependent" dispersion relations:

$$\mathbf{k}_\perp^2 - \varepsilon_1\mu_1\frac{\omega_{\mathbf{l}}^2}{c^2} = \kappa_{1l}^2, \quad \mathbf{k}_\perp^2 - \varepsilon_2\mu_2\frac{\omega_{\mathbf{l}}^2}{c^2} = \kappa_{2l}^2, \tag{14}$$

where Eq. (2) was used in each region. In cylindrical coordinates the transverse Laplacian is defined by

$$-\boldsymbol{\nabla}_\perp^2 r_{\mathbf{k}_\perp} = \mathbf{k}_\perp^2 r_{\mathbf{k}_\perp}, \tag{15}$$

with eigenvalue $\mathbf{k}_\perp^2$. In DCE experiments the slab is usually bounded by a cavity (not depicted in Fig. 1) where

$$r_{\rm np}(\mathbf{x}_\perp) = \frac{1}{\sqrt{\pi}}\frac{1}{R J_{n+1}(x_{\rm np})} J_n\left(x_{\rm np}\frac{\rho}{R}\right)e^{in\theta}, \tag{16}$$

$x_{\rm np}$ is the pth root of $J_n(x) = 0$ [22], and the fundamental cavity mode is $x_{01} = 2.4048$. For a cavity bounding the SM interface in the transverse directions we would have $R_{sp} \leqslant R = 2.5$ cm and hence $(\mathbf{k}_\perp^{\rm sp})^2 = (x_{np}/R_{\rm sp})^2 \sim O(1)$; this depends on the value of q [see Eq. (32)]. For the photon branch we always have $(\mathbf{k}_\perp^{\rm ph})^2 = (x_{np}/R)^2$ for a bounded cavity. Note in either case the mode functions are orthonormal: $(r_{\ell n}, r_{np}) = \delta_{\ell p}$.

Standard boundary conditions at an interface

$$(\mathbf{D}_2 - \mathbf{D}_1)\cdot\hat{\mathbf{z}} = 0, \quad \hat{\mathbf{z}}\times(\mathbf{E}_2 - \mathbf{E}_1) = 0 \tag{17}$$

[22] then imply $A_1 = A_2$ and

$$\frac{\kappa_1(t)}{\varepsilon_1(t)} + \frac{\kappa_2(t)}{\varepsilon_2(t)} = 0, \tag{18}$$

which requires that each dielectric be of opposite sign to generate SPPs [15]. Eliminating the z-dependent κ_i, we then find the following "electric" dispersion relation:

$$k_\perp = |\mathbf{k}_\perp| = \frac{\omega_\perp^{\rm sp}}{c}\sqrt{\frac{\varepsilon_1\varepsilon_2}{\varepsilon_1+\varepsilon_2}}\left(\frac{\varepsilon_1\mu_2 - \varepsilon_2\mu_1}{\varepsilon_1 - \varepsilon_2}\right). \tag{19}$$

[3]The x, y dependence of the mode functions decouples and can be written in terms of the index $\mathbf{l} \to l$ from now on.

With $\mu_1 = \mu_2$ we get the standard result

$$(\omega_\perp^{\rm sp})^2 = k_\perp^2 c^2\left(\frac{1}{\varepsilon_1} + \frac{1}{\varepsilon_2}\right), \tag{20}$$

where here we allow for time-dependent dielectrics, possibly in either region I or II, and $\perp = (n, p)$ because for SPPs the axial direction l is redundant. In Sec. III we will use a plasma-type model to obtain more detailed analytic properties of the above dispersion relation.

It is also worth mentioning that magnetic SPPs exist for TE modes [23]. Using the TE components of the Hertz vectors and using an equation like Eq. (13) for $\Psi(\mathbf{x},t)$ along with

$$(\mathbf{B}_2 - \mathbf{B}_1)\cdot\hat{\mathbf{z}} = 0, \quad \hat{\mathbf{z}}\times(\mathbf{H}_2 - \mathbf{H}_1) = 0 \tag{21}$$

lead again to $A_1 = A_2$ but now with

$$\frac{\kappa_1(t)}{\mu_1(t)} + \frac{\kappa_2(t)}{\mu_2(t)} = 0. \tag{22}$$

As also discussed in [23], SPPs can exist for TE modes as long as, for example, $\mu_1 < 0, \mu_2 > 0$, which can be achieved using split-ring resonators (e.g., see [15]), using fabricated metamaterials. Finally, using $\mathbf{\Pi}_m$ in Eq. (2) leads to the "magnetic" dispersion relation:

$$k_\perp = \frac{\omega_\perp^{\rm sp}}{c}\sqrt{\frac{\mu_1\mu_2}{\mu_1+\mu_2}}\left(\frac{\mu_1\varepsilon_2 - \mu_2\varepsilon_1}{\mu_1 - \mu_2}\right). \tag{23}$$

This result can be obtained from the electric sector by swapping $\varepsilon_i \leftrightarrow \mu_i$ and simplifies, when $\varepsilon_1 = \varepsilon_2$, to

$$(\omega_\perp^{\rm sp})^2 = k_\perp^2 c^2\left(\frac{1}{\mu_1} + \frac{1}{\mu_2}\right). \tag{24}$$

As also discussed in [23], this implies that TE modes can sustain surface plasmons; however, the material needs to be a fabricated metamaterial.

To compare vacuum-excited SPPs with some experimental proposals for photon creation using semiconductor slabs (e.g., see [8]), we will also consider TM modes in a slab of width $(L - a)$, placed in a cylindrical cavity of length L (not shown). These have the following orthonormal mode functions for the TM photon Hertz scalar:

$$\Phi_{\rm ph}(\mathbf{r},t) = \begin{cases} A_1\cos(k_{1l}z) r_{\rm np}(\mathbf{x}_\perp), & 0 < z < a, \\ A_2\cos(k_{2l}(L-z)) r_{\rm np}(\mathbf{x}_\perp), & a < z < L, \end{cases} \tag{25}$$

where (using the same TM interface conditions as before) we find the following transcendental equation:

$$\frac{k_{1l}\tan(k_{1l}a)}{\varepsilon_1(t)} = \frac{k_{2l}\tan(k_{2l}[a-L])}{\varepsilon_2(t)} \tag{26}$$

for the eigenvalues. This agrees with the result in [9] but can be derived with the minimum effort using Hertz vectors and can be generalized to arbitrary transverse section. Note that the photon dispersion relation (in this case for a cylindrical section) at any given time in regions I and II,

$$\omega_{i\mathbf{l}}^{\rm ph}(t) = \frac{c}{\varepsilon_i(t)}\sqrt{k_{il}^2(t) + \left(\frac{x_{\rm np}}{R}\right)^2}, \tag{27}$$

must be equal at the interface, implying equivalence of the dispersion relations:

$$\frac{1}{\varepsilon_1}\left[k_{1l}^2+\left(\frac{x_{\rm np}}{R}\right)^2\right]=\frac{1}{\varepsilon_2}\left[k_{2l}^2+\left(\frac{x_{\rm np}}{R}\right)^2\right]. \tag{28}$$

Note this dispersion relation is the complex conjugate of that in Eq. (14): $k=i\kappa$. Both this constraint and the eigenvalue relation, Eq. (26), must be simultaneously satisfied [9]. For slab thicknesses with $L-a\ll L$ (or for $a\ll L$) one can further show [9] that even for quite large variations in the dielectric constant the approximate solution to Eq. (26) is (for $l>0$)

$$k_{1l}(t)=\left(\frac{l\pi}{L}\right)\left\{1-\frac{a}{L}\left[\frac{\varepsilon_1(t)}{\varepsilon_2}-1\right]\left(\frac{x_{\rm np}}{R}\right)^2\left(\frac{L}{l\pi}\right)^2\right\} \tag{29}$$

[note TE modes at $O(a/L)$ are still unperturbed free modes [9]].

Here we ignore the zero modes, $l=0$, as previous work [17] on plasma sheets showed they are not excited; however, see discussion in [24] for dielectrics. In this case the interface constraint, Eq. (28), suggests that $k_{i0}=0$ $(i=1,2)$ implies $\varepsilon_1=\varepsilon_2$ and is therefore only satisfied for time-independent (static) cases. The general case, not just for $\eta=a/L\ll 1$, will be investigated more thoroughly elsewhere. We therefore assume TM_{011} is the lowest mode and investigate the number of created particles for this and the TE_{111} fundamental mode [up to $O(a/L)$], comparing them to that for SPPs.

III. GENERALIZED PLASMA MODEL

A. Region II: Time Independence

To simplify our analysis we will now consider a slight generalization of the plasma model [18] of a metal-like substance in region II:[4]

$$\varepsilon_2(\omega)=\bar{\varepsilon}_2\left[1-\left(\frac{\omega_p^2}{\omega^2}\right)\right], \tag{30}$$

where $\omega_p=ne^2/(\bar{\varepsilon}_2 m_*)$ is the plasma frequency, n is the number of bulk electrons, and m_* is the effective mass. The extra multiplicative factor arises by including a mass term in the Lagrangian [Eq. (1)]. In our envisaged experiment $\bar{\varepsilon}_2$ will be a constant, but for generality we have left it time dependent, $\bar{\varepsilon}_2(t)$, in the analysis below. Note the dielectric permittivity in region II takes negative values for $\omega<\omega_p$. For region I we assume a semiconductor material that is modulated by laser irradiation.

If we then substitute Eq (30) into Eq. (20) (using $\omega=\omega_\perp^{\rm sp}$), we obtain a generalization of the solution found in [23]:

$$(\omega_\perp^{\rm sp})^2=\omega_p^2\left[\frac{1}{2}+\frac{1}{2}q^2\left(\frac{1}{\varepsilon_1}+\frac{1}{\bar{\varepsilon}_2}\right)-\sqrt{\frac{1}{4}+\frac{1}{4}q^4\left(\frac{1}{\varepsilon_1}+\frac{1}{\bar{\varepsilon}_2}\right)^2+\frac{1}{2}q^2\left(\frac{1}{\bar{\varepsilon}_2}-\frac{1}{\varepsilon_1}\right)}\right], \tag{31}$$

[4]We could similarly include the magnetic permeabilities, μ_1,μ_2, but for simplicity we set them to unity.

where

$$q=\frac{k_\perp c}{\omega_p} \tag{32}$$

and we obtain the standard result for $\bar{\varepsilon}_1=\varepsilon_2=1$ [23].

We also find the following asymptotic behavior:

$$\begin{aligned}\omega_\perp^{\rm sp}&\to k_\perp c\left(\frac{1}{\varepsilon_2}\right)^{1/2}+O(q^3)+\cdots \quad q\to 0,\\ \omega_\perp^{\rm sp}&\to\frac{\omega_p}{\sqrt{2}}+O(q^{-2})+\cdots \quad q\to\infty,\end{aligned} \tag{33}$$

which explains why, for small q, we have a system that behaves like TE and TM modes in a one-dimensional cavity. Hence for a given form of modulation (see below) of the dielectric, the limit $q\to 0$ leads to parametric amplification of SPPs, while $q\to\infty$ gives no SPP production (for $\omega_p=$ const).

B. Region I: Time dependence

To be more specific, in this paper we will consider two kinds of modulation of the dielectric in region I, given that in Eq. (30) for region II.

One is an inverse sinusoidal modulation

$$\frac{1}{\varepsilon_1}=\frac{1}{2}\left(\frac{1}{\varepsilon_{1,\min}}+\frac{1}{\varepsilon_{1,\max}}\right)+\frac{1}{2}\left(\frac{1}{\varepsilon_{1,\min}}-\frac{1}{\varepsilon_{1,\max}}\right)\cos(2\omega_0 t) \tag{34}$$

that has been argued to arise from the excitation of localized electrons in a semiconductor via laser irradiation (e.g., see [24]). In this regard, we should mention that for the excitation of electrons to the conduction band, instead of using a dielectric model, such as Eq. (34), the conductivity modulates by assuming the plasma frequency varies with, for example, a sinelike time dependence, $\omega_p(t)=e^2n(t)/m_*$, where $n_s(t)\propto\sin(2\omega_0 t)$, and an equation like that in Eq. (30) but instead for region I. This is an interesting problem but differs in that $\varepsilon_1<0$ for certain modulations and will be left for future work (also see [17] for more on plasma sheet models). In this article we will assume that $\varepsilon_{1,\min},\varepsilon_{1,\max}>0$.

Another way to realistically modulate the permittivity $\varepsilon_1(t)$, but this time sinusoidally, would be to use an appropriately doped semiconductor (with two well -defined energy levels within the band gap) via Rabi oscillations (e.g., see [25]):

$$\varepsilon_1=\frac{1}{2}(\varepsilon_{1,\max}+\varepsilon_{1,\min})+\frac{1}{2}(\varepsilon_{1,\max}-\varepsilon_{1,\min})\cos(2\omega_0 t). \tag{35}$$

In the next section we shall assume that for both cases we have $\varepsilon_{1,\min}=0.2$ and $\varepsilon_{1,\max}=3.2$, which are typical values for a germanium semiconductor.

IV. PARTICLE CREATION RATES

To find the number of particles created we use an alternative to the Bogoliubov method using only mode functions [26]. We start with the quantum field operator expansion in the Heisenberg representation for our TM Hertz potential:

$$\hat{\Phi}(\mathbf{x},t)=\sum_l[\hat{a}_l\varphi_l(\mathbf{x})q_l(t)+\hat{a}_l^\dagger\varphi_l^*(\mathbf{x})q_l^*(t)], \tag{36}$$

where $\hat{a}_l, \hat{a}_l^\dagger$ are annihilation and creation operators, respectively, and the mode functions $\varphi_{\mathbf{l}}(\mathbf{x}), q_{\mathbf{l}}(t)$ were defined in Eqs. (6), (7), and (8); here we need to impose initial conditions at $t = 0$: $q_l(0) = \frac{1}{\sqrt{2\tilde{\omega}_l}}$ and $\dot{q}_l(0) = -i\sqrt{\frac{\tilde{\omega}_l}{2}}$. To find a separable time-dependent solution we can rescale the field as $\tilde{q}_{\mathbf{l}} = \varepsilon^{1/2} q_{\mathbf{l}}$ to get an equation in Mathieu form:

$$\ddot{\tilde{q}}_l + \tilde{\omega}_l^2(t)\tilde{q}_l = 0, \tag{37}$$

where

$$\tilde{\omega}_l^2 = \left[\omega_l^2 + \frac{1}{4}\frac{\dot{\varepsilon}^2}{\varepsilon^2} - \frac{1}{2}\frac{\ddot{\varepsilon}}{\varepsilon}\right]. \tag{38}$$

It may be worth mentioning that this equation is equivalent to a scalar potential in a curved space-time with conformal coupling $\xi = 1/6$ and scale factor $\varepsilon(t) = a(t)$ for a Robertson-Walker space-time [27].

The particle number density can be obtained directly from the energy of each mode divided by the energy $\tilde{\omega}_l$ of each particle:

$$n_l = \frac{\tilde{\omega}_l}{2}\left(\frac{|\dot{\tilde{q}}_l|^2}{\tilde{\omega}_l^2} + |\tilde{q}_l|^2\right) - \frac{1}{2}, \tag{39}$$

where we have subtracted off the zero point energy with units $\hbar, c = 1$. Equation (37) has a well-known structure of narrow or broad resonances for certain parameters. We stress that this method has separated variables without using an instantaneous basis approximation (see Appendix C).

Before numerically solving for the number of created particles, we will estimate the pair creation rate analytically. If the background field (the laser) leads to shifts in frequency near parametric resonance,

$$\omega_{\mathbf{m}}^2(t) \sim \omega_{0\mathbf{m}}^2 + \Delta\omega_{0\mathbf{l}}^2 = \omega_{0\mathbf{m}}^2[1 + \kappa\cos(\Omega_{\mathbf{l}} t)], \tag{40}$$

where the driving frequency is chosen as $\Omega_{\mathbf{m}} = 2\omega_{0\mathbf{m}}$, where $\mathbf{m} = (\perp, \mathbf{l})$ for SPPs and photons, respectively, then in the late-time limit,

$$n_{\mathbf{m}} \approx \sinh^2(\omega_{0\mathbf{m}}\kappa t/4), \tag{41}$$

which can be derived by ignoring second-order time derivatives in Eq. (37) [28].

As a simple example consider $\mu_1 = \mu_2$, where the time-dependent electric SPP dispersion relation (31) could be varied using a laser with driving frequency $\Omega_l = 2\omega_{0l}$ for $\bar{\varepsilon}_2 > 0$ and $\bar{\varepsilon}_2 = \text{const}$ [see Eq. (30)], with ε_1 varying inversely sinusoidally as $\varepsilon_{\min} < \varepsilon_1(t) < \varepsilon_{\max}$; then

$$\frac{\varepsilon_2}{\varepsilon_1(t)} \sim \chi + \kappa\cos(2\omega_{0l} t), \tag{42}$$

where $\chi > 0$ is an overall time-independent frequency shift [see Eq (34)]. Then Eq. (41) leads to a particle rate:

$$n_\perp^{\text{sp}} = \sinh^2\left(k_\perp^2 c^2 \frac{\kappa}{4\varepsilon_2} t\right). \tag{43}$$

This equation is also valid for the more general case of $\varepsilon_2 < 0$ not just the model discussed in Sec. III.

We can now compare this to the ω_{011} TM mode (the lowest-frequency cylindrical mode [17]), where in the limit of $(L - a) \ll L$, from Eq. (29) and equivalence of the dispersion relations [see discussion after Eq. (27)], the photon eigenvalues shift by [to order $O(a/L)$]

$$\Delta\omega_{0\mathbf{l}}^2(t) = \frac{2x_{np}^2 c^2}{R^2\varepsilon_2}\frac{a}{L}\left[\frac{\varepsilon_2}{\varepsilon_1(t)} - 1\right]. \tag{44}$$

Parametric enhancement for the photon branch is then achieved by choosing

$$\frac{\varepsilon_2}{\varepsilon_1(t)} \sim \chi + \kappa\cos(2\omega_{0l} t), \tag{45}$$

(for photons χ and κ may or may not be the same as those for SPPs). However, they are assumed to be the same magnitude. Note the resonant frequencies are not the same: $\omega_{0\perp} \neq \omega_{0\mathbf{l}}$. This leads to

$$n_{\mathbf{l}}^{\text{ph}} = \sinh^2\left(\frac{x_{np}^2 c^2}{R^2}\frac{a\kappa}{2\varepsilon_2 L} t\right). \tag{46}$$

Thus, for a cylindrical cavity the SPP creation rate dominates the photon rate if $k_\perp^2 \gg (x_{np}^2/R^2)(2a/L)$. For example, with a cavity of radius $R = 2.5$ cm and length $L = 10$ cm, for $a/L \sim O[10^{-4}]$ and $x_{01} = 2.4048$ we require that $k_\perp^2 \gg 1/25$ or $k_\perp \gg 1/5$. This is easily achieved for SPPs which have their modes bounded by a transverse section.

We have also confirmed these findings numerically by assuming both an inverse sinusoidal [see Eq. (34)] and a sinusoidal variation [see Eq. (35)] for region I (see top and bottom panels in Fig. 2, respectively). In both examples we have assumed $\varepsilon_{1,\max} = 3.2$ to $\varepsilon_{1,\min} = 0.2$, where, as we mentioned, the inverse profile is meant to model the laser irradiation of a semiconductor, while the latter one models the Rabi-like oscillations in a doped semiconductor [24]. Here we chose the transverse radial section for the dielectric slab and SPPs to be $R_{\text{sp}} = R = 2.5$ cm, the slab radius (used in $k_\perp = x_{\text{np}}/R$). It may be worth mentioning that for $q = (k_\perp c/\omega_p) \to 0$ (Zenneck waves) the propagation length becomes unbounded, but by enclosing the SM interface within a cavity of transverse section, $k_\perp$ stays bounded.

In Fig. 3 we also plot the creation rate numerically for the fundamental TE_{111} cylindrical mode for a sinusoidal variation.[5] We see that the SPP rate is of a similar magnitude for both inverse sinusoidal and sinusoidal variations, and we also see that both TM branch SPP and photons are a magnitude larger when compared to sinusoidal ones. This indicates that using doped semiconductors would lead to easier detection of pair-created photons or vacuum SPPs, although *a priori* we should consider the effects of dissipation and solve the photon eigenvalues [Eq. (26)] for general values of $\eta = a/L$ (see Sec. VI).

V. DETECTION SCHEME

In our proposed detection scheme (see Fig. 1), we have chosen region II to be that of a metal such as silver that hence satisfies $\varepsilon_2 < 0$ for frequencies blow the plasma frequency

[5]For inverse sinusoidal modulations we find that $\tilde{\omega}_{\mathbf{l}}^m$ becomes imaginary for certain times. Note that although the TE frequency is not perturbed at leading order (for $a \ll L$), the overall factor of $1/\varepsilon(t)$ [see Eq. (27)] still leads to shifts in eigenfrequency [see Eq. (38)].

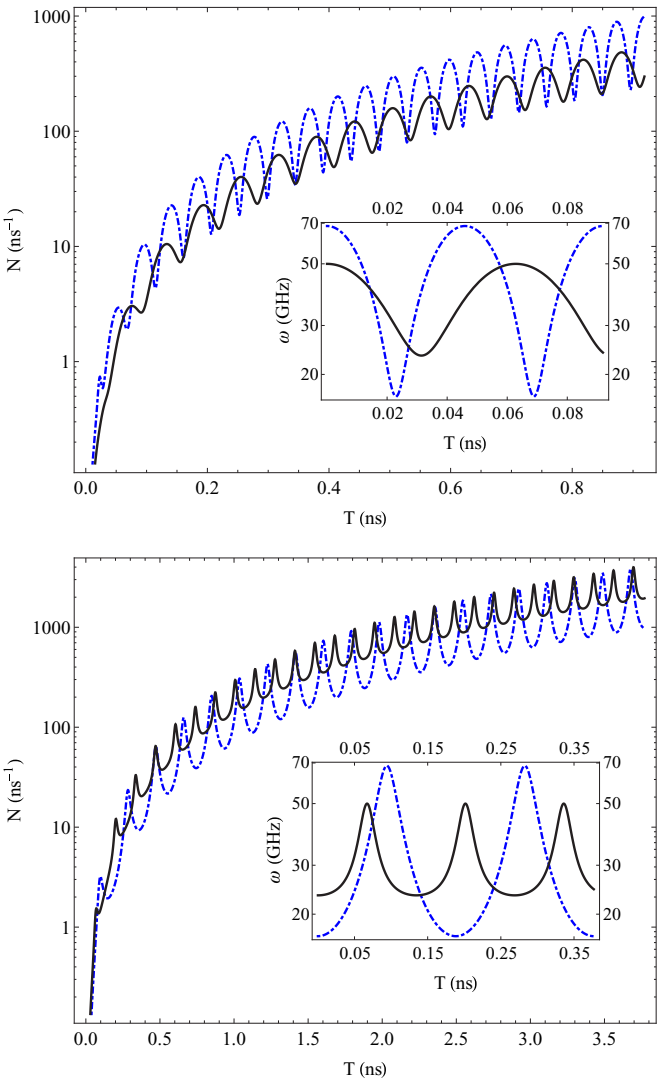

FIG. 2. (Color online) Particle creation rates for SPPs (solid-dark) and 2nd fundamental TM_{011} (dot-dashed-blue), for a pulse train of 100 pulses, $\eta = 0.01$, $R_{sp} = R = 2.5$ cm, region II, with $\bar{\varepsilon}_2 = 1.0$ and $\omega_p = 1.5 \times 10^{15}\ s^{-1}$ for silver. In region I we have (top) an inverse sinusoidal variation and (bottom) a sinusoidal variation ranging from $\varepsilon_{1,max} = 3.2$ to $\varepsilon_{1,min} = 0.2$ [see Eqs. (34) and (35)]. Insets show plots of $\omega_{\mathbf{l}}^{spp}$, ω_{011}^{phot} for each case.

ω_p [see Eq. (30)]. To realistically modulate the permittivity $\varepsilon_1(t)$, we have discussed possible inverse sinusoidal variations arising from the excitation of localized electrons below the conduction band [24] and arising from intraband transitions in a doped semiconductor [25], respectively. As we mentioned, for laser pulses with an energy $(h\lambda/c)$ above the band gap, a time-varying bulk conductivity $\rho(t)$ would be generated, leading to a modulated permittivity with $\varepsilon_{min} < 0$ (shifts $\chi < 0$), and will be left for future investigation. Hence in this article we consider only SM interfaces, such that interface region I has $\varepsilon_1(t) > 0$, and region II always has $\varepsilon_2 < 0$.

One possible way to detect vacuum-excited SPPs would be to use near-field microscopy with a photon scanning tunneling microscope (e.g., see [15]), where the microscope is placed on the opposite vacuum or air side of the SM interface, region II (see Fig. 1). Usually, to *generate* SPPs a monochromatic light

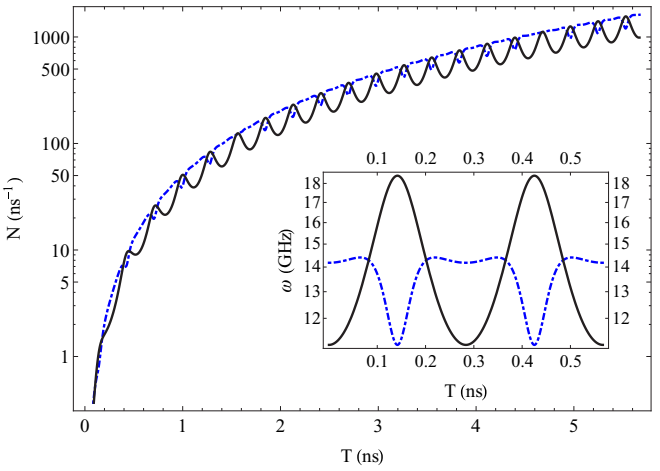

FIG. 3. (Color online) Comparison with Fig. 2 (bottom panel) for TE modes. The particle creation rate for single-mode coupling in the instantaneous basis approximation (solid black line) and the exact solution (dot-dashed blue line) for a sinusoidal variation [see Eq. (35)] for TE_{111} with the same conditions as in Fig. 2. The inset shows a comparison of $\tilde{\omega}_{111}^{phot}$ and ω_{111}^{phot}.

source is sent into a prism placed above the interface with total internal reflection at angle θ_i. The SPPs are detected by finding a decrease in emitted power at θ_i. However, the time-reversed case is equivalent to the creation of vacuum-excited SPPs and therefore would lead to a *telltale* signature: SPPs would be created via the observation of an increase in emitted power at θ_i during the time modulation of ε_1. We should, however, require that the pulsed laser itself does not generate SPPs, as can be arranged by uniformly irradiating the dielectric slab at 90° incidence (see Fig. 1).

The experimental details we mentioned so far are simple extensions of current DCE experiments [10]. However, it may well also be possible to use experiments that have already detected DCE analog radiation in metamaterials [13]. The analogy between SPPs in this work and metamaterials comes from considering flux qubits coupled to coplanar waveguides [29]. Such experimental conditions have already been demonstrated [30] by coupling artificial atoms to carbon nanotubes, and it seems within reach of current technology to also adapt these experiments to time-dependent variations of flux qubits (already done in [12,13] for photon analogs).

We can also go further with metamaterials, where say $\mu_2 < 0$, where in the late-time limit the SPP creation rate is

$$n_{\perp}^{sp} = \sinh^2\left(k_{\perp}^2 c^2 \frac{\kappa}{4\mu_2} t\right) \tag{47}$$

for

$$\frac{\mu_2}{\mu_1(t)} \sim \chi + \kappa\cos(2\omega_{0l}t). \tag{48}$$

Given that $\sinh(-x) = -\sinh x$, there is no problem in having $\mu_2 < 0$ because $n_{\perp}^{sp}$ depends quadratically on sinh.

This rate is also comparable to the photon-photon rate if μ_1 were varied in time above gigahertz frequencies. It would be interesting to try and design experiments in centimeter- or micrometer-sized cavities using split-ring resonators and wire rods that are then modulated in time.

This leads to easier detection by precisely controlling the SPP wavelength λ_{sp}.

VI. CONCLUSION AND OUTLOOK

We have discussed how SPPs can be excited out of the vacuum for the case where a dielectric crystal changes from a minimum to maximum value at a semiconductor semispace-metal (SM) interface during laser irradiation. We separated Maxwell's equations in a generalized Lorenz gauge for time-dependent media for both the permittivity and permeability. For parametric oscillations of a dielectric slab our analytic and numerical analyses show that vacuum-excited SPPs can be of the same order of magnitude as the photon-photon rate.

The results for the photon creation rate in a cylindrical cavity (generalizing the rectangular case [9]) were also found. For experimental proposals to detect DCE radiation [10], the detection of vacuum-excited SPPs has added benefits compared to photon modes: SPPs do not actually need a bounding cavity as they are planar modes (only photon modes need this for parametric enhancement), and for $\mu_i = \text{const}$, TM branch SPP and photon modes are not detuned from their resonant frequencies like TE photons.

As future work we should also include dissipative effects because even without $\text{Im}[\varepsilon] \neq 0$, it is possible to have imaginary $\tilde{\omega}$ in the photon branch. The separation of variables method used here [21] that we generalized to a Lorenz-like gauge naturally allows one to incorporate $\text{Im}[\varepsilon]$. In fact, for $\text{Im}[\varepsilon]$, the propagation length via $(2\text{Im}[k_\perp])^{-1}$ for SPPs diminishes, not the production rate, so this might lead to another benefit. These and other issues including detuning of resonant frequencies arising from dissipation will be addressed elsewhere.

It would also be interesting to investigate the vacuum excitation of volume and bulk plasmon polaritons (VPPs), usually created by firing a beam of electrons (e.g., see [31]) because longitudinal modes are not excited by light and hence require particle impact at an interface (e.g., see [15]). However, vacuum excitations might be achieved dynamically by firing clusters of "neutral" argon atoms at a sample of material [32] or by placing the sample on a high-frequency piezo (e.g., see [33]). The issue of the gap between bulk and surface plasmons [31] indicates they are more difficult to create.

Finally, for time-dependent media, it has recently been suggested [20] that not only transverse (TE and TM) modes but also longitudinal modes can be created out of vacuum. These are usually *unphysical* in Gupta-Bleuler quantization due to a cancellation among time and longitudinal components. However, the authors of [20] argue that for a time-dependent permittivity $\varepsilon(t)$ such a cancellation does not occur and surface charges arise as a real physical effect from longitudinal modes. The issue of quantization in general time-dependent media requires further investigation, where it would be interesting to find the relationship, or difference, between vacuum-excited SPPs and possible surface charges from longitudinal modes.

Note added. We have become aware of another paper dealing with the spontaneous emission of photon pairs from a metamaterial junction [34]. However, we consider instead the *stimulated emission* of photon pairs from nonadiabatic changes in the vacuum state. We have also recently come across a work with ideas similar to those given here: that surface plasmons can be created out of vacuum excitations at a time-modulated interface [35].

ACKNOWLEDGMENTS

We thank Y. Kido (Ritsumeikan University), R. Johansson (RIKEN), G. S. Paraoanu (Aalto University School of Science), and H. Tagawa (Fujitsu) for useful discussions on surface plasmons, quantum circuits, flux qubits, and separation of variables, respectively.

APPENDIX A: TIME-DEPENDENT BACKGROUNDS

Here we discuss a convenient way to separate Maxwell's equations using Hertz vectors. This was developed by Nisbet [19] for nondispersive inhomogeneous time-dependent media. Here we generalize to the case of an isotropic and time-dependent medium.[6]

Maxwell's equations in SI units are

$$\begin{aligned} \nabla\cdot\mathbf{B} = 0, \quad \nabla\times\mathbf{E} = -\dot{\mathbf{B}}, \\ \nabla\cdot\mathbf{D} = \rho, \quad \nabla\times\mathbf{H} - \dot{\mathbf{D}} = \mathbf{J}, \end{aligned} \tag{A1}$$

where

$$\mathbf{D} = \varepsilon(t,\mathbf{x})\mathbf{E}, \quad \mathbf{B} = \mu(t,\mathbf{x})\mathbf{H}. \tag{A2}$$

In the above we have assumed both zero permanent polarization and magnetization ($\mathbf{P}_0 = \mathbf{M}_0 = 0$), and later we will also assume zero bulk charges and currents ($\rho = 0, \mathbf{J} = 0$), although for now we keep them to see how general Maxwell's equations can remain in order to separate them.

We now define the electromagnetic fields in terms of gauge potentials as follows:

$$\mathbf{B} = \nabla\times\mathbf{A}, \quad \mathbf{E} = -\partial_t\mathbf{A} - \nabla A_0, \tag{A3}$$

where upon substitution into Maxwell's equations (A1) we find that Gauss's and Ampere's laws lead to

$$\begin{aligned} -\nabla\cdot\left(\varepsilon\frac{\partial}{\partial t}\mathbf{A}\right) - \nabla\cdot(\varepsilon\nabla A_0) = \rho, \\ \frac{\partial}{\partial t}\left(\varepsilon\frac{\partial}{\partial t}\mathbf{A}\right) + \frac{\partial}{\partial t}(\varepsilon\nabla A_0) + \nabla\times\left(\frac{1}{\mu}\nabla\times\mathbf{A}\right) = \mathbf{J}. \end{aligned} \tag{A4}$$

At this point separation of these coupled equations requires some assumptions to be made. The separation in the Coulomb gauge was achieved in the seminal paper by Dodonov *et al.* [28] assuming a factorizable ansatz: $\varepsilon(\mathbf{r},t) = \varepsilon(t)\varepsilon(\mathbf{x})$ and $\mu(\mathbf{r},t) = \mu(t)\mu(\mathbf{x})$.

The separation is more difficult in the Lorenz gauge; however, Nisbet [19] was able to separate Maxwell's equations using what we shall call a generalized spatial Lorenz gauge:

$$\mu\varepsilon\partial_t(A_0) + \nabla\cdot[\varepsilon(\mathbf{x})\mathbf{A}] = 0, \tag{A5}$$

assuming time-independent media, which is not the standard Lorenz gauge. For the case of time-dependent media, a

[6]Time dependent in both the permittivity and permeability.

generalized temporal Lorenz gauge can be found:

$$\mu(t)\partial_t(\varepsilon(t)A_0) + \boldsymbol{\nabla}\cdot\mathbf{A} = 0, \tag{A6}$$

which works as long as we assume an isotropic piecewise homogeneous and time-dependent media: $\varepsilon(t),\mu(t)$, and $\nabla\mu = \nabla\varepsilon = 0$ (see [20] for the case of $\mu = 1$). Note a generalized spatiotemporal Lorenz gauge of the form $\mu(t)\partial_t(\varepsilon(t)A_0) + \boldsymbol{\nabla}\cdot(\varepsilon(\mathbf{x})\mathbf{A})$ does not lead to a complete separation, which can be verified. However, the separation of a nondispersive, inhomogeneous, conducting, and time-dependent medium assuming a factorizable geometry (see [28]) appears to be possible and will be presented elsewhere.

Plugging the temporal Lorenz gauge, Eq. (A6), into Eq. (A4), assuming $\nabla\varepsilon = \nabla\mu = 0$, leads to two uncoupled second-order differential equations of the form

$$\begin{aligned}\frac{\partial}{\partial t}\left(\mu\frac{\partial}{\partial t}(\varepsilon A_0)\right) - \nabla^2 A_0 &= \frac{\rho}{\varepsilon},\\ \mu\frac{\partial}{\partial t}\left(\varepsilon\frac{\partial}{\partial t}\mathbf{A}\right) - \nabla^2\mathbf{A} &= \mu\mathbf{J},\end{aligned} \tag{A7}$$

which generalizes the result found in [20] when $\mu = 1$. The above result also generalizes work in the Coulomb gauge by Dodonov *et al.* [28] and work in [9], which considered either time-dependent ε or μ using dual potentials and hence does not allow for the inclusion of charge and current densities which break the duality [22] (also see [21] for time-dependent media in the Coulomb gauge).

Note that Eqs. (A7) are not symmetric in an interchange of $\varepsilon \leftrightarrow \mu$, which is due to the nontrivial time dependence of the media. However, a symmetric set of equations (with respect to $\varepsilon \leftrightarrow \mu$) can be obtained from the Hertz method, as we show in Appendix B.

APPENDIX B: HERTZ VECTORS

We now define two Hertz vectors $\boldsymbol{\Pi}_e$ and $\boldsymbol{\Pi}_m$ as (with $\mu_0 = 1$)

$$A_0 = -\frac{1}{\varepsilon}\boldsymbol{\nabla}\cdot\boldsymbol{\Pi}_e, \quad \mathbf{A} = \mu\frac{\partial\boldsymbol{\Pi}_e}{\partial t} + \boldsymbol{\nabla}\times\boldsymbol{\Pi}_m, \tag{B1}$$

which automatically satisfies the temporal Lorenz gauge condition, Eq. (A6) (see [19] for the definition of potentials on a spatial Lorenz gauge). It is then possible to show that the coupled wave equation, Eq. (A7), separates as

$$\begin{aligned}\varepsilon(t)\partial_t(\mu(t)\partial_t\boldsymbol{\Pi}_e) - \nabla^2\boldsymbol{\Pi}_e &= \mathbf{Q}_e,\\ \mu(t)\partial_t(\varepsilon(t)\partial_t\boldsymbol{\Pi}_m) - \nabla^2\boldsymbol{\Pi}_m &= \mathbf{Q}_m,\end{aligned} \tag{B2}$$

where TE modes correspond to $\boldsymbol{\Pi}_m$, while TM modes are for $\boldsymbol{\Pi}_e$ [for more details see discussion following Eq. (2)]. Here we have included the so-called stream potentials [19],

$$\begin{aligned}\boldsymbol{\nabla}\cdot\mathbf{Q}_e &= -\rho,\\ \dot{\mathbf{Q}}_e + \frac{1}{\mu}\boldsymbol{\nabla}\times\mathbf{Q}_m &= \mathbf{J},\end{aligned} \tag{B3}$$

set to zero in the main text as we assume that $\rho,\mathbf{J} = 0$ [see Eq. (2)]. It may also be worth mentioning that these equations are slightly different from the case discussed in [23] that applies to a dispersive medium, $\varepsilon(\omega),\mu(\omega)$, on a time-independent ($e^{i\omega t}$) background.

The electric and magnetic fields can then be written in terms of Hertz vectors as

$$\begin{aligned}\mathbf{E} &= \frac{1}{\varepsilon}\boldsymbol{\nabla}(\boldsymbol{\nabla}\cdot\boldsymbol{\Pi}_e) - \partial_t(\mu\,\partial_t\boldsymbol{\Pi}_e) - \boldsymbol{\nabla}\times\partial_t\boldsymbol{\Pi}_m\\ &= \frac{1}{\varepsilon}\boldsymbol{\nabla}\times(\boldsymbol{\nabla}\times\boldsymbol{\Pi}_e) - \boldsymbol{\nabla}\times\partial_t\boldsymbol{\Pi}_m,\\ \mathbf{B} &= \mu\boldsymbol{\nabla}\times\frac{\partial\boldsymbol{\Pi}_e}{\partial t} + \boldsymbol{\nabla}\times(\boldsymbol{\nabla}\times\boldsymbol{\Pi}_m),\end{aligned} \tag{B4}$$

allowing one to easily isolate TE and TM modes.

For example, TM modes are defined by the parts $\mathbf{E}_{\mathrm{TM}},\mathbf{B}_{\mathrm{TM}}$ coming from $\boldsymbol{\Pi}_e$ with $\mathbf{z}\cdot\mathbf{B} = 0$, where a convenient choice of Hertz vectors is

$$\boldsymbol{\Pi}_e = \Phi\,\hat{\mathbf{z}}, \qquad \boldsymbol{\Pi}_m = \Psi\,\hat{\mathbf{z}}$$

and Φ and Ψ represent TM and TE modes, respectively. For TM modes we obtain

$$\begin{aligned}\mathbf{E}_{\mathrm{TM}} &= \frac{1}{\varepsilon}\partial_1\partial_z\Phi\hat{\mathbf{e}}_1 + \frac{1}{\varepsilon}\partial_2\partial_z\Phi\hat{\mathbf{e}}_2,\\ \mathbf{B}_{\mathrm{TM}} &= \mu\,\partial_2\partial_t\Phi\hat{\mathbf{e}}_1 - \mu\,\partial_1\partial_t\Phi\hat{\mathbf{e}}_2,\end{aligned} \tag{B5}$$

with a similar expression for TE modes (from $\boldsymbol{\Pi}_m$ with $\mathbf{z}\cdot\mathbf{E} = 0$):

$$\begin{aligned}\mathbf{E}_{\mathrm{TE}} &= -\partial_2\partial_t\Psi\hat{\mathbf{e}}_1 + \partial_1\partial_t\Psi\hat{\mathbf{e}}_2,\\ \mathbf{B}_{\mathrm{TE}} &= \partial_1\partial_z\Psi\hat{\mathbf{e}}_1 + \partial_2\partial_z\Psi\hat{\mathbf{e}}_2.\end{aligned} \tag{B6}$$

These generalize the time-independent cases found, e.g., in [23].

These equations, of course, combine for both TE and TM modes to give the total electric and magnetic field strengths:

$$\begin{aligned}\mathbf{E} &= \left(\frac{1}{\varepsilon}\partial_1\partial_z\Phi - \partial_2\partial_t\Psi\right)\hat{\mathbf{e}}_1 + \left(\frac{1}{\varepsilon}\partial_2\partial_z\Phi + \partial_1\partial_t\Psi\right)\hat{\mathbf{e}}_2\\ &\quad - \frac{1}{\varepsilon}\boldsymbol{\nabla}_\perp^2\Phi\,\hat{\mathbf{z}},\\ \mathbf{B} &= (\mu\,\partial_2\partial_t\Phi + \partial_1\partial_z\Psi)\,\hat{\mathbf{e}}_1 + (-\mu\,\partial_1\partial_t\Phi + \partial_2\partial_z\Psi)\,\hat{\mathbf{e}}_2\\ &\quad - \boldsymbol{\nabla}_\perp^2\Psi\,\hat{\mathbf{z}},\end{aligned} \tag{B7}$$

and they generalize the time-independent case (e.g., see [23]) to the time-dependent case.

APPENDIX C: SEPARATION OF VARIABLES IN TIME-DEPENDENT MEDIA

To allow for space-time-dependent mode functions we can also use an instantaneous basis [36]:

$$\Phi(\mathbf{r},t) = \sum_m Q_{\mathbf{m}}(t)\varphi_{\mathbf{m}}(\mathbf{r};t), \tag{C1}$$

where now t becomes a parameter: $\varphi(\mathbf{r},t) \to \varphi(\mathbf{r};t)$. The orthonormality again is given by

$$\int_0^L dz\,\varepsilon(t)\varphi_{\mathbf{m}}(\mathbf{r};t)\varphi_{\mathbf{n}}(\mathbf{r};t) = (\varphi_{\mathbf{m}},\varphi_{\mathbf{n}}) = \delta_{\mathbf{mn}} \tag{C2}$$

and satisfies the wave equation

$$\nabla^2\varphi_{\mathbf{m}}(\mathbf{r};t) + \varepsilon(t)\mu(t)\omega_{\mathbf{m}}^2(t)\varphi_{\mathbf{m}}(\mathbf{r};t) = 0. \tag{C3}$$

These steps appear to be identical to the standard separation of variables; however, the time-dependent wave equation now

becomes [36] [see Eq. (8)]

$$\ddot{Q}_{\mathbf{m}} + \omega_{\mathbf{m}}^2(t) Q_{\mathbf{m}} = -\sum_{\mathbf{m}}^{\infty} \left[2M_{\mathbf{mn}} \dot{Q}_{\mathbf{n}} + \dot{M}_{\mathbf{mn}} Q_{\mathbf{n}} + \sum_{\ell}^{\infty} M_{\mathbf{nl}} M_{\mathbf{ml}} Q_{\mathbf{n}} \right] = 0 \quad \forall \quad M_{\mathbf{mn}} \to 0, \tag{C4}$$

where the intermode coupling matrix is given by

$$\mathcal{M}_{\mathbf{mn}} = \int_0^L dz\, \varepsilon(t) \varphi_{\mathbf{m}}(\mathbf{r};t) \partial_t \varphi_{\mathbf{n}}(\mathbf{r};t), \tag{C5}$$

and for a crystal in free space the bounds would be $\pm\infty$.

That is, the instantaneous basis approximation assumes that the variable t becomes a parameter, such that we can freeze time derivatives of $\dot{\varepsilon} = \ddot{\varepsilon} = 0$ (or μ). On the other hand, in the usual separation of variables [see Eq. (8)], the time derivatives remain, but a rescaling of the mode functions allows us to find a Mathieu-like solution [see Eq. (37)]. As we shall see, in the instantaneous approach, instead of these terms we obtain an infinite set of coupled mode equations.

Upon substituting the mode expansion for the instantaneous basis into the Lagrangian density, Eq. (1), and then integrating over the spatial part using the orthonormality of the mode functions, defining the conjugate momentum as

$$\Pi(\mathbf{r},t) = \varepsilon(t) \sum_{\mathbf{m}} P_{\mathbf{m}}(t) \varphi_{\mathbf{m}}(\mathbf{r};t), \tag{C6}$$

we obtain, via a Legendre transform, a Hamiltonian of the form [37]

$$H_{\text{eff}} = \sum_{\mathbf{m}} \left[P_{\mathbf{m}}^2 + \omega_{\mathbf{m}}^2(t) Q_{\mathbf{m}}^2 \right] + \sum_{\mathbf{mn}} P_{\mathbf{m}} Q_{\mathbf{n}} \mathcal{M}_{\mathbf{mn}}(t). \tag{C7}$$

Now the conjugate momentum is defined by

$$P_{\mathbf{m}} = \dot{Q}_{\mathbf{m}} - \mathcal{M}_{\mathbf{mn}} Q_{\mathbf{n}}. \tag{C8}$$

Only in special cases does the intermode coupling matrix, Eq. (C5), become zero, such as for certain cavity geometries or for a uniform dielectric filling the whole cavity ($a = L$) [36]. However, in general, both methods introduce detuning of the parametric enhancement. In the separation of variables this comes from the shifted dispersion relation $\tilde{\omega}_{\mathbf{l}}(t)$, while in the instantaneous basis it comes from the intermode coupling term $\mathcal{M}_{\mathbf{mn}}(t)$.

Specifically, it is important to note that for SPPs considered here, the definition in Eq. (13) implies there are no intermode coupling terms: $\mathcal{M}_{\mathbf{mn}} = 0$ as imposed by the orthonormality of the SPPs. Hence the instantaneous basis leads to a single mode equation which is identical to only the separation of variables approach for $\dot{\varepsilon}, \ddot{\varepsilon} = 0$. This is exemplified by the fact that the frequencies do not depend on time derivatives of ε in the instantaneous basis method [see Eq. (8)]: $\tilde{\omega}^{\text{sp}} \neq \omega^{\text{sp}}$ (see the inset in Fig. 3).

[1] J. S. Schwinger, On gauge invariance and vacuum polarization, Phys. Rev. **82**, 664 (1951).

[2] L. Parker, Particle creation in expanding universes, Phys. Rev. Lett. **21**, 562 (1968).

[3] S. Hawking, Black hole explosions, Nature (London) **248**, 30 (1974).

[4] P. D. Nation, J. R. Johansson, M. P. Blencowe, and F. Nori, *Colloquium*: Stimulating uncertainty: Amplifying the quantum vacuum with superconducting circuits, Rev. Mod. Phys. **84**, 1 (2012).

[5] D. Allor, T. D. Cohen, and D. A. McGady, Schwinger mechanism and graphene, Phys. Rev. D **78**, 096009 (2008).

[6] G. L. Klimchitskaya and V. M. Mostepanenko, Creation of quasiparticles in graphene by a time-dependent electric field, Phys. Rev. D **87**, 125011 (2013).

[7] G. T. Moore, Quantum theory of the electromagnetic field in a variable-length one-dimensional cavity, J. Math. Phys. **11**, 2679 (1970).

[8] V. Dodonov, Current status of the dynamical casimir effect, Phys. Scr. **82**, 038105 (2010).

[9] M. Uhlmann, G. Plunien, R. Schützhold, and G. Soff, Resonant cavity photon creation via the dynamical casimir effect, Phys. Rev. Lett. **93**, 193601 (2004).

[10] A. Agnesi, C. Braggio, G. Bressi, G. Carugno, F. Della Valle, G Galeazzi, G. Messineo, F. Pirzio, G. Reali, G. Ruoso, D. Scarpa, and D. Zanello, MIR: An experiment for the measurement of the dynamical casimir effect, J. Phys.: Conf. Ser. **161**, 012028 (2009).

[11] E. Segev, B. Abdo, O. Shtempluck, E. Buks, and B. Yurke, Prospects of employing superconducting stripline resonators for studying the dynamical casimir effect experimentally, Phys. Lett. A **370**, 202 (2007).

[12] C. M. Wilson, G. Johansson, A. Pourkabirian, M. Simoen, J. R. Johansson, T. Duty, F. Nori, and P. Delsing, Observation of the dynamical casimir effect in a superconducting circuit, Nature (London) **479**, 376 (2011).

[13] P. Lähteenmäki, G. S. Paraoanu, J. Hassel, and P. J. Hakonen, Dynamical casimir effect in a Josephson metamaterial, Proc. Natl. Acad. Sci. U.S.A. **110**, 4234 (2013).

[14] M. F. Maghrebi, R. L. Jaffe, and M. Kardar, Spontaneous emission by rotating objects: A scattering approach, Phys. Rev. Lett. **108**, 230403 (2012).

[15] S. A. Maier, *Plasmonics: Fundamentals and Applications* (Springer, New York, 2007).

[16] F. Intravaia and A. Lambrecht, Surface plasmon modes and the casimir energy, Phys. Rev. Lett. **94**, 110404 (2005).

[17] W. Naylor, Towards particle creation in a microwave cylindrical cavity, Phys. Rev. A **86**, 023842 (2012).

[18] T. Kawakubo and K. Yamamoto, Photon creation in a resonant cavity with a nonstationary plasma mirror and its detection with Rydberg atoms, Phys. Rev. A **83**, 013819 (2011).

[19] A. Nisbet, Electromagnetic potentials in a heterogeneous non-conducting medium, Proc. R. Soc. London, Ser. A **235**, 375 (1957).

[20] X.-M. Bei and Z.-Z. Liu, Quantum radiation in time-dependent dielectric media, J. Phys. B **44**, 205501 (2011).

[21] I. A. Pedrosa and A. Rosas, Electromagnetic field quantization in time-dependent linear media, Phys. Rev. Lett. **103**, 010402 (2009).
[22] J. D. Jackson, *Classical Electrodynamics*, 3rd ed. (Wiley, New York, 1998).
[23] V. V. Nesterenko and I. G. Pirozhenko, Lifshitz formula by a spectral summation method, Phys. Rev. A **86**, 052503 (2012).
[24] M. Uhlmann, Dynamical casimir effect: Photon production in a cavity with a time-dependent medium slab, Diploma thesis, Dresden University, 2004.
[25] H. Haug and S. W. Koch, *Quantum Theory of the Optical and Electronic Properties of Semiconductors*, 4th ed. (World Scientific, Singapore, 2004).
[26] L. Kofman, A. Linde, and A. A. Starobinsky, Towards the theory of reheating after inflation, Phys. Rev. D **56**, 3258 (1997).
[27] N. D. Birrell and P. C. W. Davies, *Quantum Fields in Curved Space* (Cambridge University Press, Cambridge, 1982).
[28] V. V. Dodonov, A. B. Klimov, and D. E. Nikonov, Quantum phenomena in nonstationary media, Phys. Rev. A **47**, 4422 (1993).
[29] G. S. Paraoanu, Fluorescence interferometry, Phys. Rev. A **82**, 023802 (2010).
[30] O. Astafiev, A. M. Zagoskin, A. A. Abdumalikov, Yu. A. Pashkin, T. Yamamoto, K. Inomata, Y. Nakamura, and J. S. Tsai, Resonance fluorescence of a single artificial atom, Science **327**, 840 (2010).
[31] H. Raether, *Surface Plasmons on Smooth Surfaces* (Springer, Berlin, 1988).
[32] N. Inui, K. Mochiji, and K. Moritani, Actuation of a suspended nano-graphene sheet by impact with an argon cluster, Nanotechnology **19**, 505501 (2008).
[33] W.-J. Kim, J. H. Brownell, and R. Onofrio, Detectability of dissipative motion in quantum vacuum via superradiance, Phys. Rev. Lett. **96**, 200402 (2006).
[34] S. Ghosh and S. K. Maiti, Spontaneous photoemission from metamaterial junction: A Conjecture, arXiv:1306.3748.
[35] V. Hizhnyakov, A. Loot, and S. Azizabadi, Dynamical casimir effect for surface plasmon polaritons, Phys. Lett. A **379**, 501 (2015).
[36] C. K. Law, Effective hamiltonian for the radiation in a cavity with a moving mirror and a time-varying dielectric medium, Phys. Rev. A **49**, 433 (1994).
[37] R. Schutzhold, G. Plunien, and G. Soff, Trembling cavities in the canonical approach, Phys. Rev. A **57**, 2311 (1998).